RSC Advances

ROYAL SOCIETY OF CHEMISTRY

www.rsc.org/advances

RSC Advances RSCPublishing

PAPER

Temperature Effects on Nano-porous $ZnCo_2O_4$ Anode with Excellent Capability for Li-ion Batteries

Cite this: *RSC Advances*, 2015, xx, xx

Ji-Xuan Fu, Wei-Ting Wong and Wei-Ren Liu*

Received 00th xx 2015,
Accepted 00th xx 2015

DOI: 10.1039/x0xx00000x

www.rsc.org/advances

In this study, nano-porous $ZnCo_2O_4$ anode are synthesized via a hydrothermal method with subsequently different annealing temperature. X-ray diffraction (XRD), Brunauer-Emmett-Teller (BET), scanning electron microscopy (SEM), and transmission electron microscopy (TEM) are carried out to study the crystal structure, pore size distribution, surface morphology and characteristics, respectively. With increasing the sintering temperature, the morphology of $ZnCo_2O_4$ turns to sphere-like with porous structure. The as-prepared porous $ZnCo_2O_4$ nanospheres synthesized at optimal condition of 600 ^oC (ZCO-600) demonstrates high capacity of 1800 mAh/g and good retention performance of 1242 mAh/g after 30 cycles. The AC data shows that the ZCO-600 anode gives lower impedance compared to ZCO with other temperature. The porous nanosturcture and large surface area are responsible for superior performance. Moreover, nano-porous ZCO synthesized at 500 ^oC better cycle performance and excellent rate capability than other synthetic temperature of 600 ^oC and 700 ^oC, because of their superiority properties in structure.

1. Introduction

In recent years, Lithium-ion batteries (LIBs) extensively apply on many electronic applications like portable electronic devices, electric vehicles (EVs), hybrid electric vehicles (HEVs), energy storage systems (ESSs), and so forth because of their high energy density, perfect lifespan and environmentally friendly.[1-4] To develop the high energy capacity, long cycle life and low environmental impact materials of LIBs used in above devices becomes very important.[5]

In aspects of anode materials, graphite is the primary one used in market. However, the theoretical capacity of commercial graphite anode is just only 372 mAh g^{-1}, which cannot meet our demand for high energy capacity in the future.[6] Therefore, it is necessary to look for the better materials to replace the graphite. In recently research, 3D transition metal oxides with nanostructure and porous characterize have been found in good at improving cycle performance and coulombic efficiency with high capacity.[7-10]

On previous reports, these transition metal oxides such as NiO,[11] Fe_2O_3[12] and Co_3O_4[13] have shown the excellent electrochemical performance. Among all of them, Co_3O_4 exhibits the best anodic performance with high theoretical capacity as high as ~900 mAh g^{-1}.[1, 14-21] However, cobalt is toxic and expensive thus it is unfriendly to our environment and the commercial costs are too high to bear. In order to solve above disadvantages, cobalt are being made to partially replace Co_3O_4 with eco-friendly and cheaper alternative metals such as Ni,[10] Zn,[22] Mg,[23] Fe[23] and Mn[24, 25], which are also electrochemically active for Li insertion and extraction. The spinel anode materials have been reported on $NiCo_2O_4$,[27, 28] $ZnCo_2O_4$,[29-34] $MgCo_2O_4$,[23] $FeCo_2O_4$,[23] $MnCo_2O_4$/$CoMn_2O_4$,[24,35] and $CuCo_2O_4$.[36] Among all of them, $ZnCo_2O_4$ has strong potential as an electrode material for lithium storage and could provide the highest capacity because both Zn and Co are more electrochemically active with respect lithium than other alternative metals.[37] Therefore, $ZnCo_2O_4$ is considered as the most attractive material to substitute for graphite anode in Li-ion battery due to its perfect electrochemical properties such as high reversible capacity, perfect cycle performance and good environmental protection.[34]

So far, with different shape $ZnCo_2O_4$ nanomaterials have been widely studied, such as nanoparticles[29], nanoflakes[38], nanotubes[37], nanowires[39] and nanorods[40], prepared by different method all exhibited excellent electrochemical performances. However, little literature focus on the synthetic temperature on the structural change and electrochemical performance.

Thus, in this study, we attempt to systematically synthesize ZCO with different annealing temperature from 500 ^oC to 700 ^oC. The corresponding characterizations, including different electrochemical analyses and BET measurements to firstly establish the relationship between structure and electrochemical properties. The results could be an important information for material design of ZCO a potential anode for Li-ion batteries in the future.

2. Experimental section

2.1. Preparation of the electrode materials

The sphere-like $ZnCo_2O_4$ with porous nanostructure was synthesized by using hydrothermal method. Typically, 0.5425 g

of zinc oxide (ZnO, 99.5%, SIGMA-ALDRICH) was dissolved in ~5 mL dilute nitric acid (HNO_3, 65%, SIGMA-ALDRICH) and 60 mL DI water to get the solution. Then added 3.8805 g of cobalt nitrate ($Co(NO_3)_2 \cdot 6H_2O$, 98%, SHOWA) and 0.8406 g of citric acid ($C_6H_8O_7 \cdot 1H_2O$, 99.5%, SIGMA-ALDRICH) to dissolved in the above solution under continuous stirring for 10 min and the pH was adjusted to 7 by adding ammonium hydroxide (NH_4OH, 25%, FISHER). The mixture solution was subsequently transferred to a 100 mL Teflon-lined stainless steel autoclave. The autoclave was heated to 180 °C for 24 h. After heating, the autoclave was air-cooled to room temperature and the resulting pink precipitate was washed with DI water for several times and then dried at 80 °C. The precipitate were separately annealed at 500 °C, 600 °C and 700 °C for 3 h to obtain the final products.

2.2. Material characterization

The products were characterized by powder X-ray diffraction (XRD, Bruker D8 Advance Eco) with Cu Kα radiation (λ= 1.5418Å). The thermogravimetric analysis (TGA/DTG, TA Q50) measurements of the $ZnCo_2O_4$ precursors were carried out at a heating rate of 5 °C min^{-1} from room temperature to 800 °C. The morphology and structure of the products were analysed by scanning electron microscopy (SEM, Hitachi S-4100) and transmission electron microscopy (TEM), then element mapping by energy-dispersive X-ray spectroscopy (EDS).The Brunauer-Emmett-Teller (BET) surface area and pore size were tested by using Micromeritics Tristar 3000.

2.3. Electrochemical measurements

The electrochemical performance of the products were measured by using CR2032 coin cells. The working electrode was composed of 60 wt.% active materials, 25 wt.% KS-6, 5 wt.% super-P, 6 wt.% CMC and 4 wt.% SBR, coating on the 10 μm copper foil, then dried at 120°C for 8 h in vacuum system to remove the residual water. The electrolyte consisted of 1M $LiPF_6$ in ethylene carbonate (EC) and ethyl methyl carbonate (EMC) (1:1 in volume ratio). The discharge/charge test was analysed by AcuTech System in the voltage range of 0.01-3.5 V at room temperature. The mass loading of these sample is in the range of 2.4 ~ 4 mg/cm^2. The Cyclic voltammograms (CV) were measured by CH Instruments Analyzer CHI 6273E at a scan rate of 0.001 mVs^{-1} between 0.01 V and 3.5 V, then tested the AC impedance in the frequency range from 1 Hz ~ 100000 Hz.

3. Results and discussion

Figure 1 shows the XRD patterns of $ZnCo_2O_4$ synthesized by different annealing temperature of 500 °C, 600 °C and 700 °C. All the diffraction peaks at 2θ values of 18.89°, 31.29°, 36.84°, 38.51°, 44.82°, 55.67°, 59.35°, 65.26° and 72.28° which corresponding respectively to the diffraction planes (111), (220), (311), (220), (400), (422), (511) and (440), respectively. All these diffraction peaks match well with the cubic spinel structure with XRD database in JCPDS-23-1390. Absence of any diffraction peak of Co_3O_4 and ZnO, confirmed the high purity of the products, and the schematic crystal structure of spinel $ZnCo_2O_4$ was demonstrated. Furthermore, based on the full width at half maximum of diffraction peak (311), the crystal size of the products was calculated using Scherrer's equation: $D = \kappa\lambda/\beta 1/2\cos\theta$, where κ is shape factor, β is the line broadening at half the maximum intensity, and $\cos\theta$ is the Bragg angle. All the calculated average crystal size of the $ZnCo_2O_4$ synthesized at 500 °C and 600 °C were about 24 nm, but when the annealing temperature increased to 700 °C, the average crystal size became about 37 nm. It might be resulted from the fusion between nanoparticles with each other in higher temperature.

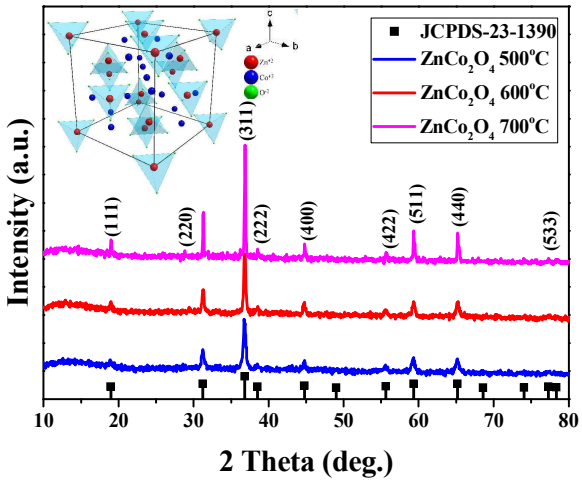

Figure 1. XRD pattern of the $ZnCo_2O_4$ synthesized at 500 °C, 600 °C and 700 °C.

Figure 2 shows the TGA and DTG results of the thermal properties of the precursor. There are two obvious weight loss during heat process. The first one occurred below 200 °C was attributed to the loss of free water or other organic molecules, while the second one was due to the thermal decomposition of the precursors into $ZnCo_2O_4$ by releasing CO_2, corresponding to sharp exothermic peaks located at 188.3 °C and 242.7 °C in the DTG curve. The large total weight loss of 54.7%, and no weight loss and exothermic peaks are found over 300 °C, indicated that precursor is transformed to $ZnCo_2O_4$ completely. Therefore, to ensure that the $ZnCo_2O_4$ obtained after annealing was pure phase, above 500 °C was chosen as the annealing temperature for the synthesis of $ZnCo_2O_4$.

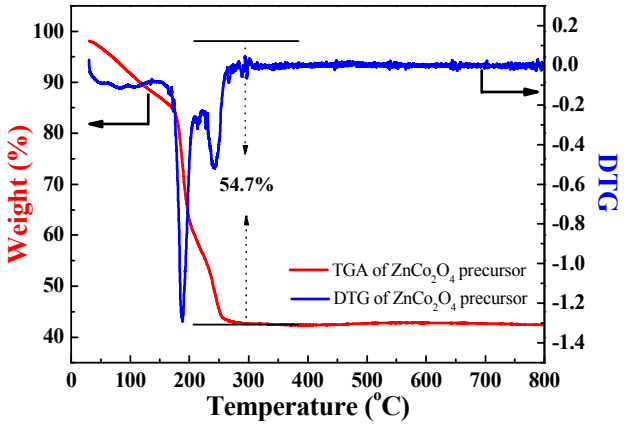

Figure 2. TGA/DTG curves for the $ZnCo_2O_4$ precursor.

Figure 3 shows the SEM images of $ZnCo_2O_4$ synthesized by different annealing temperature of 500 °C, 600 °C and 700 °C. It can be seen from Fig. 3 (a) that the structure consists of $ZnCo_2O_4$ nanoparticles with diameters of 20~30 nm, but hardly confirmed the shape of the structure in lower synthetic temperature of 500 °C. With increasing the annealing temperature to 600 °C, shown in Fig. 3 (b), the nanoparticles assemble to sphere-like structure. For higher temperature of 700 °C, it can be seen that the sphere-like structure become rough and larger because of the fusion between the nanoparticles. At the high-magnification images from Fig. 3(d) to 3 (f), all of them give porous nature, especially in 600°C. Obviously, for higher temperature of 700°C, phenomenon of sintering occur and most of these pores disappear. The porosity of ZCO, indeed, could be controlled by tuning the annealing temperature. The electrochemical properties, such as capacity, cycling stability as well as rate performance will be different. Nano sized particles with highly porosity could be a good thing for enhancing Li-ion intercalation and diffusion into the spinel lattice. It also become much easier for electrolyte penetration into the active material, thus enhancing contact areas between the electrolyte and $ZnCo_2O_4$ and shorting the Li-ion diffusion distance in the structure. Figure 4(a) shows the $ZnCo_2O_4$ synthesized at 600 °C, the diameters of $ZnCo_2O_4$ particles are about 20~30 nm, which match well with SEM observation. The HRTEM image of ZCO shown in Fig. 4(b) reveals a lattice fringe with interplane spacing of 0.25 nm, corresponding to the (311) plane of spinel $ZnCo_2O_4$ phase. From the result of SAED shown in Fig. 4(c), the *d* values of 0.286 nm, 0.244 nm and 0.202 nm were corresponding well to miller index of (220), (311) and (400) for $ZnCo_2O_4$ crystal. The EDS information of $ZnCo_2O_4$ is shown in Fig. 5(a). The elements Zn, Co and O can only be seen in the nanostructure, indicating the formation of pure phase $ZnCo_2O_4$. Figure 5(b) also shows the EDS mapping results, the elements Zn, Co and O are evenly distributed all over the structure.

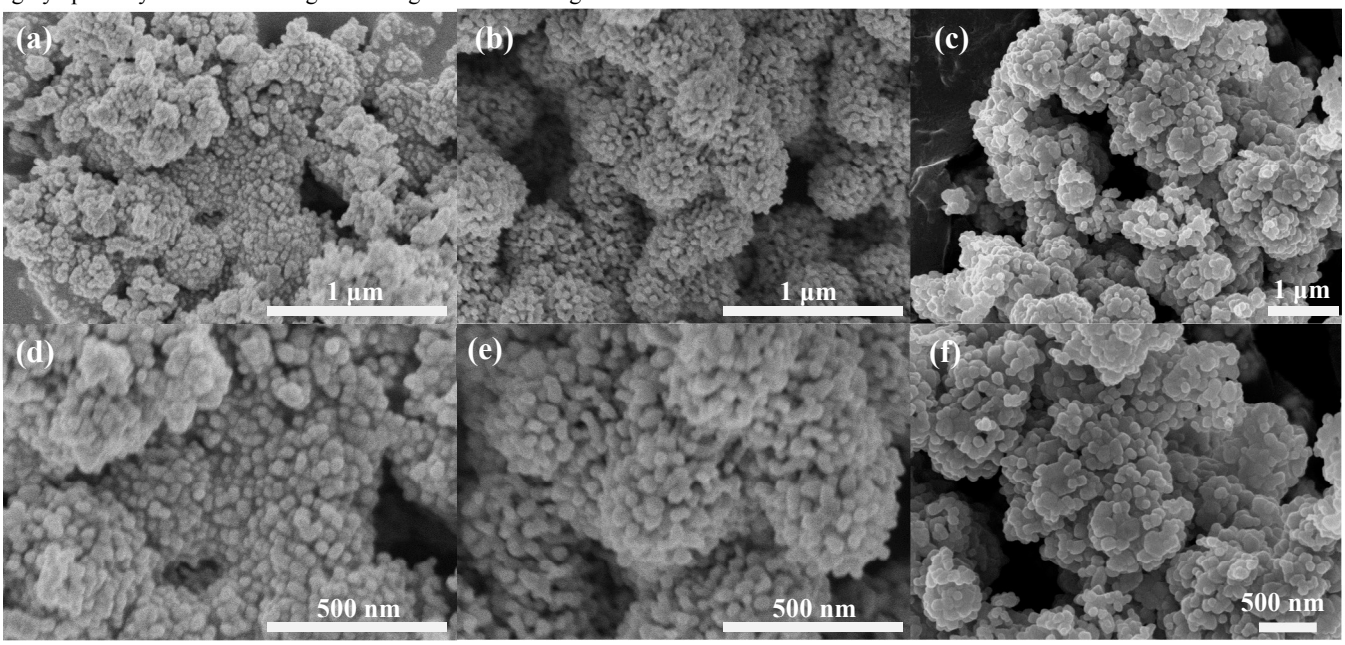

Figure 3. SEM images of $ZnCo_2O_4$ synthesized by different annealing temperature: low magnification of (a) 500 °C; (b) 600 °C; (c) 700 °C ; high magnification of (d) 500 °C; (e) 600 °C; (f) 700 °C.

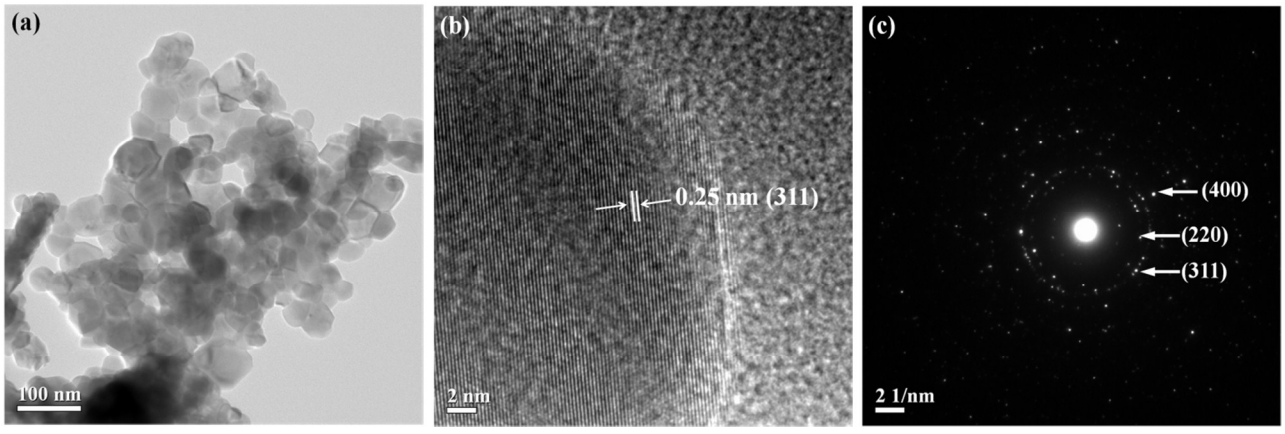

Figure 4. (a) TEM image; (b) HRTEM image; (c) SAED pattern of $ZnCo_2O_4$ synthesized at 600 °C.

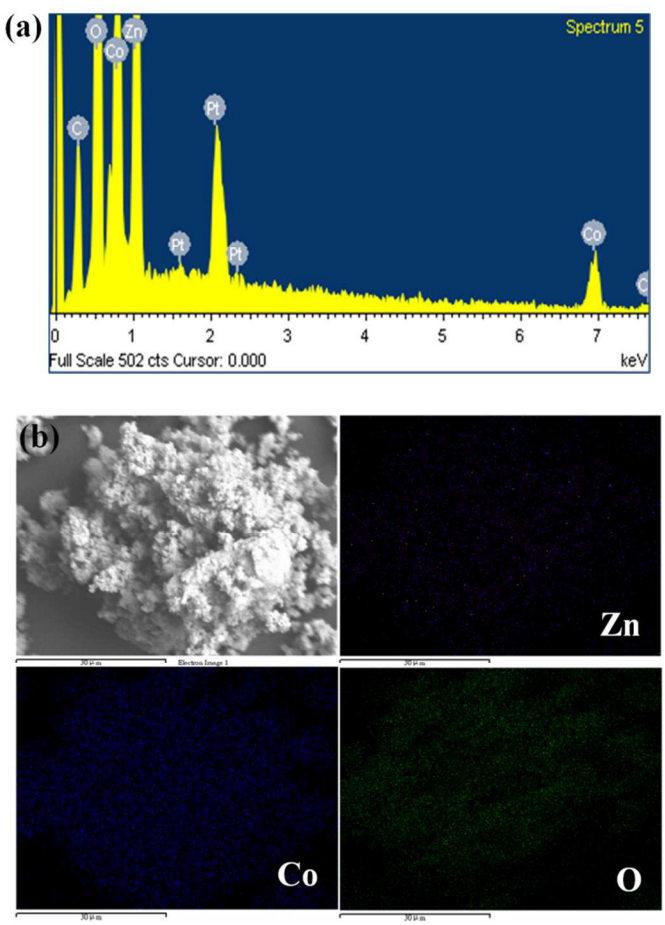

Figure 5. (a) EDS analysis; (b) EDS mapping of as-prepared $ZnCo_2O_4$.

The specific surface areas and pore size distribution of $ZnCo_2O_4$ nanosphere synthesized at different annealing temperature were characterized by BET analysis using nitrogen adsorption-desorption, as shown in Fig. 6. It can be seen that the specific surface areas of $ZnCo_2O_4$ synthesized at 500 ^oC and $ZnCo_2O_4$ synthesized at 600 ^oC are about 11.67 $m^2 g^{-1}$ and 12.48 $m^2 g^{-1}$, respectively. The specific surface area of ZCO-600 was similar to that of ZCO-500. As for ZCO-700 shown in Fig. 6(c), its specific surface area is only 7.81 $m^2 g^{-1}$. The decrease of surface area from 500-600 ^oC to 700 ^oC might be due to the fusion between the $ZnCo_2O_4$ nanoparticles at annealing higher temperature. All these ZCO showed a narrow pore size distribution below 10 nm because nano-sized $ZnCo_2O_4$ particles were formed in pores. The enhanced surface area of ZCO-500 and ZCO-600 could be attributed to smaller diameters and larger quantities of nanoparticles and nanopores.

According to the previous study, the entire electrochemical process can be explained as follow:

$$ZnCo_2O_4 + 8\ Li^+ + 8\ e^- \rightarrow Zn + 2\ Co + 4\ Li_2O \quad (1)$$

$$Zn + Li^+ + e^- \leftrightarrow LiZn \quad (2)$$

$$Zn + Li_2O \leftrightarrow ZnO + 2\ Li^+ + 2\ e^- \quad (3)$$

$$2Co + 2Li_2O \leftrightarrow 2CoO + 4\ Li^+ + 4\ e^- \quad (4)$$

$$2CoO + 2/3Li_2O \leftrightarrow 2/3Co_3O_4 + 4/3\ Li^+ + 4/3\ e^- \quad (5)$$

With the above electrochemical process, the cyclic voltammetry test (CV) and charge/discharge test can be discussed clearly below.

Figure 7(a) shows the cyclic voltammograms of ZCO-600 in the first three cycles. The reduction peak in the first cycle shows an intense irreversible reaction at ~0.15 V, which might be due to the decomposition of $ZnCo_2O_4$ to Zn^0 and Co^0 according to equation (1) with the formation of a solid electrolyte interphase (SEI). Compared with the discharge of the second and third cycle, the peaks found at ~0.4 V and ~0.7 V, indicative of different electrochemical reactions occurs at two process. However, the first three cycle all can observe two oxidation peaks at ~1.9 V and 2.3 V in the anodic polarization, which can be attributed to the oxidation of Zn^0 to Zn^{2+} and Co^0 to Co^{3+} (equation 3-5) respectively. To compare the charging/discharge degree of Li-ion in $ZnCo_2O_4$ at different annealing temperature, the CV curves of these samples in the third cycle was tested and shown in Fig. 7(b). It can be observed that the position of redox peaks for ZCO-500 and ZCO-600 was quite close, which demonstrate a similar phenomenon for Li ion diffusion in these porous structure and similar specific surface area shown in BET data. The potential of reduction reaction of ZCO-600 and ZCO-500 occur at ~1.2 V vs. Li/Li^+. However, for ZCO-700 sample, obvious polarization phenomenon was observed in CV tests. First, the current of reduction and oxidation for ZCO-700 were lower than those of ZCO-500 and ZCO-600. Second, the inset potential for reduction decrease to 0.9 V vs. Li/Li^+. The difference of electrochemical properties might be due to diffusion issue. From the view point of diffusion, nano-sized and porous nature of ZCO-500 and ZCO-600 samples provide short diffusion path of Li ion into the materials. For ZCO-700, however, lower specific surface area and pore volume might be resulted in problem in charge and discharge processes.

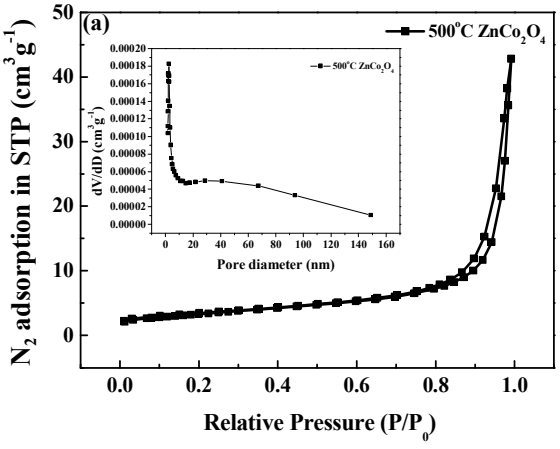

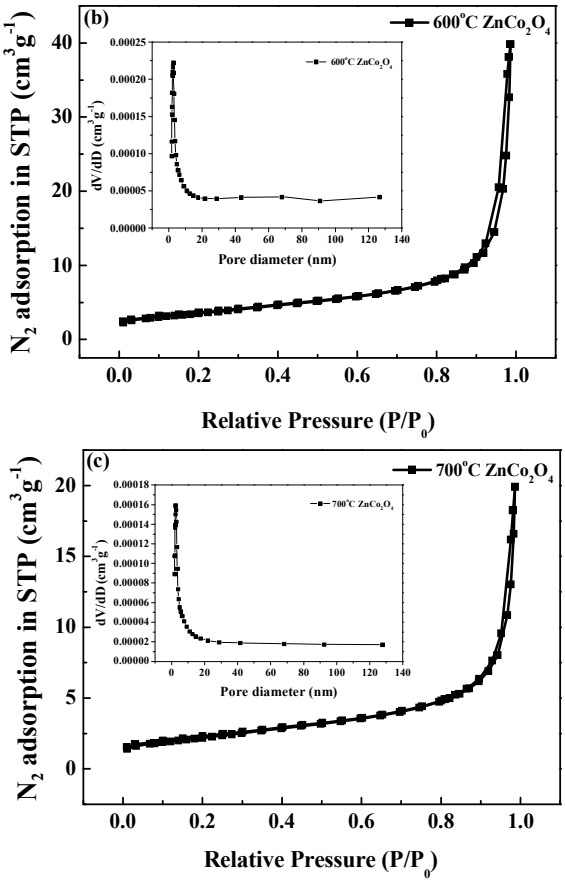

Figure 6. N_2 adsorption-desorption isotherms and BJH pore size distributions of $ZnCo_2O_4$ synthesized at (a) 500 °C; (b) 600 °C and (c) 700 °C.

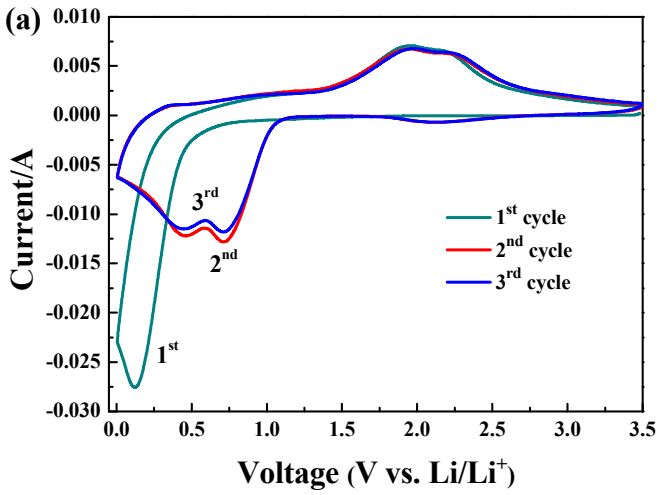

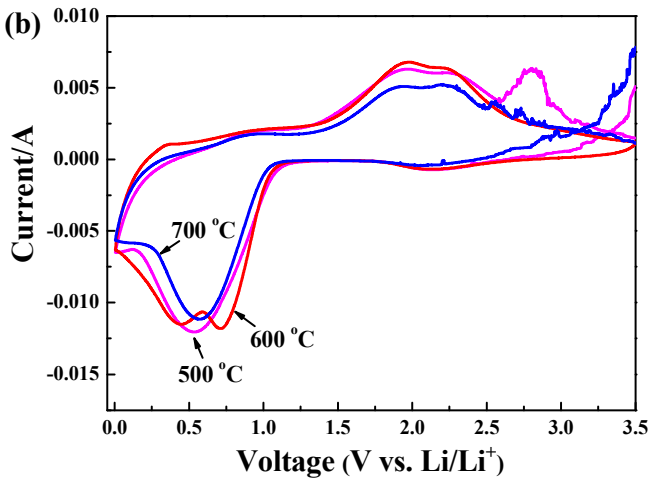

Figure 7. (a) The first three cycles of CVs for the $ZnCo_2O_4$ synthesized at 600 °C; (b) CV curves of $ZnCo_2O_4$ synthesized at 500 °C, 600 °C and 700 °C in the 3rd cycle.

Figure 8 shows charge/discharge curves of $ZnCo_2O_4$ synthesized at 600 °C at current density of 0.1 C in the voltage range of 0.01-3.5 V in the first three cycle. It can clearly be discovered that a plateau at ~0.9 V was in the first charging process. For the second and third cycle, the plateau shifts to ~1.2 V and becomes steeper, which was in consist with the CV results shown in Fig. 7(a). The initial charge and discharge capacity are 1800 and 1452 mAh/g, respectively. The coulombic efficiency in the first cycle is as high as 80.6%. The irreversible capacity loss in the first cycle is ~ 19.4%, which was associated with the formation of SEI film. In addition, the coulombic efficiency of the second cycle and third cycle enhance as high as 98.9% and 98.8%, and the charge/discharge curves almost overlap, indicating that the highly reversibility electrochemical properties of ZCO-600 and the result well match with the CV results shown before.

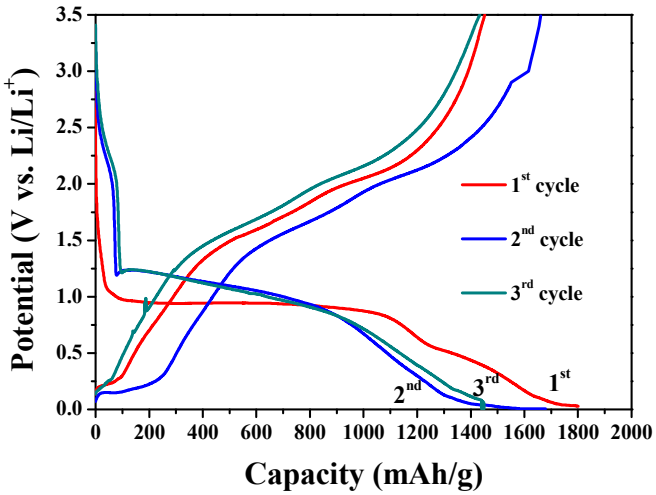

Figure 8. First three cycles discharge/charge curves of $ZnCo_2O_4$ synthesized at 600 °C.

Figure 9(a) shows the cycle performance of $ZnCo_2O_4$ synthesized at 500 °C, 600 °C and 700 °C at current density of 0.1 C. It can be observed that the initial charge/discharge capacity of the ZCO-600 is the highest one compared to ZCO-700 and ZCO-500. The change of capacity indicated that the capacity of 600 °C and 700 °C $ZnCo_2O_4$ started to decline after 12 cycles, but the capacity of 500 °C $ZnCo_2O_4$ not only did not decline but also increased, exhibited the more perfect cycle performance. After 30 cycles, the reversible capacities of 500 °C, 600 °C and 700 °C $ZnCo_2O_4$ are 1075, 1242 and 713 mAh/g, respectively. Among these sample, both ZCO-500 and ZCO-600 still retained the higher capacity and good retention, it might be attributed to the porous nanosphere structure. The BET results shown in Fig. 6, the more complete structure and higher surface area of ZCO-500 and ZCO-600 provide Li-ion the shorter diffusion distance and enhance contact areas between the electrolyte and $ZnCo_2O_4$, exhibited better capacity retained ability than other annealing temperature. The columbic efficiency of ZCO-500, ZCO-600 and ZCO-700 in the first 30 cycles, shown in Fig. 9(a), shows closed to 100% efficiency for these samples, which indicates their good cyclability. For larger current tests, Fig. 9(b) demonstrate 100 cycle tests at 1C for these three samples. Obviously, ZCO-500 gave much superior cycling performance to those of other samples. The reversible capacity of ZCO-500 could be maintain to ~500 mAh/g which is ~1.34 times than that of graphite anode.

Rate performance of ZCO in different annealing temperature is also carried out in Fig. 9(c). As shown in Fig. 9(c), the average discharge capacity of ZCO-600 decreases from ~1250, ~1100, ~950 and ~1000 mAh/g with increasing the current from 1C, 2C, 5C, and 10C. In the subsequent cycle, the capacity rebound to ~1100 mAh/g with the current back to 1C. For ZCO-500, however, demonstrate excellent capacity than that of ZCO-600 and ZCO-700. Under 10C, the capacity of ZCO-500 was as high as ~900 mAh/g. The results demonstrate again, nano structure play a very important roles in both cycle stability and rate capability.

The AC impedance results of ZCO synthesized at 500 °C, 600 °C and 700 °C after charging at the third cycle shown in Fig. 10. The diameters of the semicircles for ZCO-500, ZCO-600 and ZCO-700 are 320 Ω, 160 Ω and 725 Ω, respectively. ZCO-600 sample exhibited the lowest impedance. In order to understand the major contribution of impedance in these three samples. We use a typical equivalent circuit shown in the inset in Fig. 10. Herein, R_1, R_{SEI} and R_{CT} are impedances resulted from electrolyte, SEI film and charge transfer of ZCO, respectively. Some of the corresponding fitting data are displayed in Table 1. First of all, R_1 values for these three samples are almost the same, which was due to the similar impedance of interface between electrode and electrolyte. For the contribution of SEI film, as shown in Table 1, the R_{SEI} values were also very close because of the surface chemistry of ZCO in different annealing temperature were similar. Obviously, the dramatically difference in impedance was charge transfer resistance. The R_{CT} of ZCO-500, ZCO-600 and ZCO-700 were 243, 84.5 and 602, respectively. Thanks for the nano-porous nature, which facilities both the reaction kinetics and diffusion of Li ion.

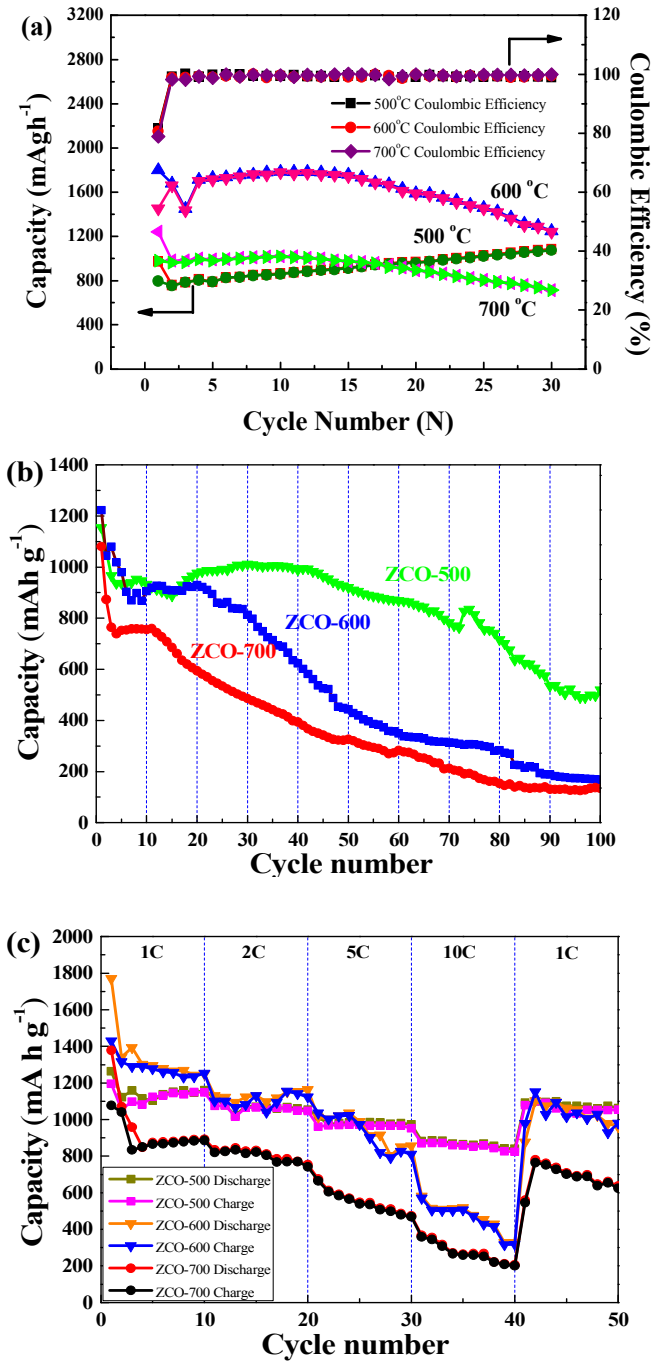

Figure 9. (a) Cycle performance of $ZnCo_2O_4$ synthesized at 500 °C, 600 °C and 700 °C for 30 cycles at 0.1C; (b) Cycle performance of $ZnCo_2O_4$ synthesized at 500 °C, 600 °C and 700 °C for 100 cycles at 1C; (c) rate performance of $ZnCo_2O_4$ synthesized at 500 °C, 600 °C and 700 °C.

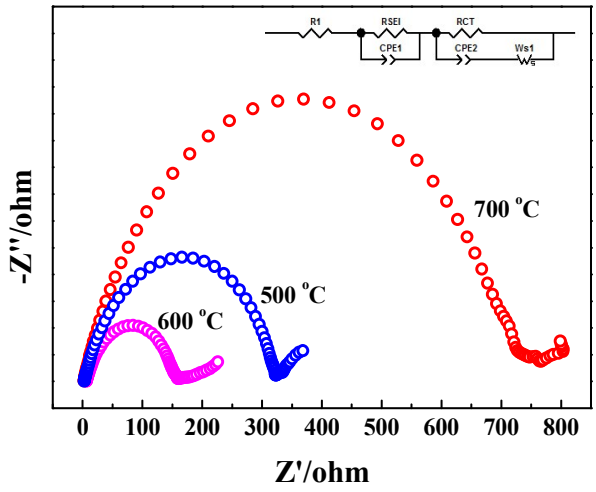

Figure 10. AC impedance of $ZnCo_2O_4$ synthesized at 500 °C, 600 °C and 700 °C at the three cycle.

Based on the above results, $ZnCo_2O_4$ synthesized at 600 °C could provide the best electrochemical properties. To exhibit the superiority of $ZnCo_2O_4$ anode materials in this study, table 2 shows the synthesis method, electrochemical properties and annealing temperature of previous research. Compared with this study, it can clearly observed that the 1st cycle discharge capacity and the 30th cycle charge capacity are all superior to related references, exhibited the excellent electrochemical properties.

Table 1. Impedance parameters calculated from equivalent circuit model.

$ZnCo_2O_4$	R_1	R_{SEI}	R_{CT}
500 °C	2.801	66	243
600 °C	2.236	62	84.5
700 °C	2.738	64	602

Table 2. Comparison of $ZnCo_2O_4$ anode materials in different groups.

Synthesis method	Morphology	1st cycle discharge capacity (mAh/g)	30th cycle charge capacity (mAh/g)	Annealing temperature	Reference
Hydrothermal method	nanospheres	1800	1242	600 °C	This study
Hydrothermal method	parallel columns	1332	~900	400 °C	[30]
Hydrothermal method	microspheres	1087	~810	700 °C	[33]
Co-precipitation	nanowires	1331	~1100	500 °C	[39]
Hydrothermal method	nanorods	1509	~850	N/A	[40]
Hydrothermal method	flower-like	1430	~895	400 °C	[41]
Co-precipitation	nanoflakes	1458	~1200	500 °C	[42]

4. Conclusions

In this study, nano-porous $ZnCo_2O_4$ anode with large surface area are successfully synthesized via a hydrothermal method. The SEM and TEM images show that the $ZnCo_2O_4$ nanosphere with diameters about 20-30 nm could be obtained. The BET results show that ZCO-500 and ZCO-600 can provide the larger surface area. The initial charge capacity of 600 °C $ZnCo_2O_4$ can reach as high as 1800 mAh/g, which was attributed to the short diffusion distances and large surface area provided by the nanostructure. After 30 cycles, the reversible capacity still retained 1242 mAh/g. The rate performance test indicates that ZCO-500 deliver the highest capacity of as high as ~900 mAh/g at 10C rate. The AC impedance results future prove that ZCO-600 gave the lowest surface layer resistance. The major enhancement of impedance was resulted from charge transfer resistance. All the results reveal that via tuning the synthetic temperature, the nano-porous $ZnCo_2O_4$ anode are expected to be a potential anode material for Li-ion batteries in the future.

Acknowledgments

The authors would like to thanks the financial support by National Science Council under contract no. of NSC-101-3113-P-002-026.

Note and references

Department of Chemical Engineering, Chung Yuan Christian University, Taiwan

1 P. Poizot, S. Grugeon, L. Dupont and J. M. Tarascon, *Nature*, 2000, **407**, 496-499.
2 Y. G. Li, B. Tan and Y. Y. Wu, *Nano Lett.*, 2008, **8**, 265-270.

3 H. L. Wang, L. F. Cui, Y. Yang, H. S. Casalongue, J. T. Robinson, Y. Y. Liang, Y. Cui and H. J. Dai, *J. Am. Cham. Soc.*, 2010, **132**, 13978-13980.
4 L. W. Ji, Z. Lin, M. Alcoutlabi and X. W. Zhang, *Energy Environ. Sci.*, 2011, **4**, 2682-2699.
5 M. C. Qiu, L. W. Yang, X. Qi, J. Li and J. X. Zhong, *ACS Appl. Mater. Interfaces*, 2010, **2(12)**, 3614-3618.
6 J. M. Tarascon and M. Armand, *Nature*, 2001, **414**, 359-379.
7 G. X. Wang, H. Liu, J. Liu, S. Z. Qiao, G. Q. Max Lu and P. Munroe, H. Ahn, *Adv. Mater.* 2010, **22**, 4994.
8 J. Chen, X. H. Xia, J. P. Tu, Q. Q. Xiong, Y. H. Yu, X. L. Wang and C. D. Gu, *J. Mater. Chem.* 2012, **22**, 15056-15061.
9 Y. F. Deng, Q. M. Zhang, Z. C. Shi, L. J. Han, F. Peng and G. H. Chen, *Electrochim. Acta*, 2010, **8**, 2828-2832.
10 L. Jingfa, X. Shenglin, L. Yurong, J. Zhicheng and Q. Yitai, *ACS Appl. Mater. Interfaces*, 2013, **5**, 981-988.
11 A. K. Mondal, D. W. Su, Y. Wang, S. Q. Chen and G. X. Wang, *Chem. Asian J.*, 2013, **8**, 2828-2832.
12 L. Zhang, H. B. Wu, R. Xu and X. W. (David) Lou, *CrystEngComm*., 2013, **15**, 9332-9335.
13 N. Jayaprakash, W. D. Jones, S. S. Moganty and L. A. Archer, *J. Power Sources*, 2012, **200**, 53-58.
14 W. -Y. Li, L. -N. Xu and J. Chen, *Adv Funct. Mater.*, 2005, **15**, 851.
15 X. W. Lou, D. Deng, J. Y. Lee, J. Feng and L. A. Archer, *Adv. Mater.*, 2008, **20**, 258.
16 S. L. Xiong, C. Z. Yuan, X. G. Zhang and Y. T. Qian, *Chem. Eur. J.*, 2009, **15**, 5320.
17 C. C. Li, X. M. Yin, T. H. Wang and H. C. Zeng, *Chem. Mater.*, 2009, **21**, 4984.
18 X. Wang, X. L. Wu, Y. G. Guo, Y. T. Zhong, X. Q. Cao, Y. Ma and J. N. Yao, *Adv. Funct. Mater.*, 2010, **20**, 1680.
19 Y. Wang, H. J. Zhang, L. Lu, L. P. Stubbs, C. C. Wong and J. Y. Lin, *ACS Nano*, 2010, **4**, 4753.
20 S. L. Xiong, J. S. Chen, X. W. Lou and X. C. Zeng, *Adv. Funct. Mater.*, 2012, **22**, 861.
21 X. L. Xiao, X. F. Liu, H. Zhao, D. F. Chen, Z. Liu, J. H. Xiang, Z. B. Hu and Y. D. Li, *Adv. Mater.*, 2012, **24**, 5762.
22 C. C. Ai, M. C. Yin, C. W. Wang and J. Sun, *J. Mater. Sci.*, 2004, **39**, 1077-1079.
23 Y. Sharma, N. Sharma, G. V. S. Rao and B. V. R. Chowdari, *Solid State Ionics*, 2008, **179**, 587-597.
24 J. F. Li, S. L. Xiong, X. W. Li and Y. T. Qian, *Nanoscale*, 2013, **5**, 2045-2054.
25 H. Liu and J. Wang, J. Electron. *Mater.*, 2012, **41(11)**, 3107-3110.
26 Y. Sharma, N. Sharma, G. V. S. Rao and B. V. R. Chowdari, *J. Power Sources*, 2007, **173**, 495-501.
27 R. Alcantara, M. Jaraba, P. Lavela and J. L. Tirado, *Chem. Mater.* 2002, **14**, 2847.
28 J. F. Li, S. L. Xiong, Y. R. Liu, Z. C. Ju and Y. T. Qian, *ACS Appl. Mater. Interfaces*, 2013, **5**, 981.
29 Y. Sharma, N. Sharma, G. V. Subba Rao and B. V. R. Chowdari, *Adv. Funct. Mater.* 2007, **17**, 2855.
30 D. Deng and J. Y. Lee, *Nanotechnology*, 2011, **22**, 355401.
31 N. Du, Y. F. Xu, H. Zhang, J. X. Yu, C. X. Zhai and D. R. Yang, *Inorg. Chem.*, 2011, **50**, 3320.
32 Y. C. Qiu, S. H. Yang, H. Deng, L. M. Jin and W. S. Li, *J. Mater. Chem.*, 2010, **20**, 4439.
33 L. L. Hu, B. H. Qu, C. C. Li, Y. J.Chen, L. Mein, D. N. Lei, L. B. Chen, Q. H. Li and T. H. Wang, *J. Mater. Chem. A*, 2013, **1**, 5596.
34 B. Liu, J. Zhang, X. F. Wang, G. Chen, D. Chen, C. W. Zhou and G. Z. Shen, *Nano Lett.*, 2012, **12**, 3005.
35 L. Hu, P. Zhang, H. Zhong, X. R. Zheng, N. Yan and Q. W. Chen, *Chem. Eur. J.*, 2012, **18**, 15049.
36 W. Kang, Y. Tang, W. Li, Z. Li, X. Yang and J. Xu, C. S. Lee, *Nanoscale*, 2014, **6**, 6551-6556.
37 L. Wei, H. Xianluo, S. Yongming and H. Yunhui, *J. Mater. Chem.*, 2012, **22**, 8916-8921.
38 Q. Yongcai, Y. Shihe, D. Hong, J. Limin and L. Weishan, *J. Mater. Chem.*, 2010, **20**, 4439-4444.
39 D. Ning, X. Yanfang, Z. Hui, Y. Jingxue, Z. Chuanxin and Y. Deren, *Inorg. Chem.*, 2011, **50**, 3320-3324.
40 H. Liu and J. Wang, *Electrochim. Acta*, 2013, **92**, 371-375.
41 S. G. Mohamed, T. F. Hung, C. J. Chen, C. K. Chen, S. F. Hu, R. S. Liu, K. C. Wang, X. K. Xin, H. M. Liu, A. S. Liu, M. H. Hsieh and B. J. Lee, *RSC Adv.*, 2013, **3**, 20143-20149.
42 X. Song, Q. Ru, B. Zhang, S. Hu and B. An, *Journal of Alloys and Compounds*, 2014, **585**, 518-522.

Ji-Xuan Fu, Wei-Ting Wong and Wei-Ren Liu*

RSC Adv. **2015**, *xx*, XXXX

Temperature Effects on Nano-porous $ZnCo_2O_4$ Anode with Excellent Capability for Li-ion Batteries

$ZnCo_2O_4$ is synthesized via a hydrothermal method with different annealing temperature. Via controlling sintering technique, the rata capability of as-prepared porous $ZnCo_2O_4$ anode is as high as ~900 mAh/g at 10C.